Near-surface electrons and acoustic phonons: Energy and momentum relaxation

Yuri M. Sirenko* and K. W. Kim
Department of Electrical and Computer Engineering, North Carolina State University, Raleigh, North Carolina 27695-7911

Michael A. Stroscio
U.S. Army Research Office, P.O. Box 12211, Research Triangle Park, North Carolina 27709-2211
(Received 20 June 1997)

We study energy and momentum relaxation of a two-dimensional (2D) electron channel located at a finite distance ℓ from a free crystal surface. The interaction with a complete set of bulklike, totally reflected, and Rayleigh acoustic phonon modes is taken into account. In most cases of interest the relaxation rates have the same temperature dependence as for 2D or bulk electrons interacting with bulk phonons. Numerical calculations demonstrate that the presence of a surface results in approximately a 10% modification of scattering rates in the high-temperature region. In the opposite limit (Bloch-Grüneisen regime), the contribution of the surface phonons may dominate over that of bulklike modes. Oscillations of the relaxation rates as a function of the distance ℓ between the electron channel and the surface are also predicted. [S0163-1829(97)01148-X]

I. INTRODUCTION

During the past decade much effort has been devoted to the understanding of the influence of spatial quantization on the vibrational properties of semiconductor heterostructures and superlattices. While optical-phonon confinement has been analyzed in great detail,[1] it is only recently that much attention has been focused on the more subtle effects of acoustic-phonon quantization in restricted geometries.[2]

The procedure of spatial quantization of acoustic waves in inhomogeneous media is quite straightforward. First, the elasticity theory equations are solved in conjunction with the proper boundary conditions to obtain the spectrum and displacement pattern of the resulting acoustic modes. For most geometries, the solutions of elastic wave equations are well established[3,4] and the studies focus on the modification of elastic modes in *ad hoc* systems. Next, the *phonon* modes are defined by applying the second quantization formalism to a complete orthonormal set of classical waves.[5] The introduction of a carrier-phonon interaction Hamiltonian facilitates the study of phonon-limited mobility, power dissipation, and other kinetic properties of confined electrons.

Depending on the system geometry, it is convenient to distinguish between buried heterostructures and self-supported structures. In *buried* waveguides and resonators, the modification of propagating bulk phonon modes results from the difference in elastic constants (sound velocities) of the materials forming a heterojunction. In narrow regions of phonon frequency ω and wave vector q evanescent waves may be supported in one or both materials, giving rise to confined and interface modes localized in the vicinity of a waveguide.[6] Thus confinement effects for *acoustic* phonons in buried structures are much weaker than for dispersionless *optical* phonons, where confined modes always exist due to the difference in the optical-phonon frequencies of the two materials.[1,2]

Early works on the acoustic wave properties of buried heterostructures were devoted primarily to the study of acoustic mode folding in superlattices.[7] Later, Tamura and co-workers investigated the resonant transmission of acoustic wave packets in superlattices and double-barrier systems.[8] Kochelap and Gülseren[9] have modeled the localization of acoustic modes due to electron-phonon interactions within a two-dimensional electron gas. Acoustic wave confinement in spherical microcrystals embedded in an elastic matrix has been studied by means of low-frequency Raman scattering.[10,11] Wendler and Grigoryan investigated the existence of interface acoustic modes in semiconductor sandwich structures[12] and Nishiguchi studied in detail the modes supported by a buried cylindrical wire.[13] Finally, we note the recent studies of elastic wave modes supported by cytoskeletal filaments and microtubules immersed in a liquid.[14]

Very recently, Nishiguchi applied the standard quantization procedure to determine both the extended and localized acoustic modes in a system of a GaAs wire embedded in an AlAs matrix.[15] The resulting phonon modes were used to calculate electron-phonon scattering rates due to the deformation potential coupling. Calculations for a wire of radius 50 Å demonstrated that the maximum contribution of confined phonons to the scattering rate is two orders of magnitude smaller than that of the extended phonons. Since the interaction with confined modes occurs only above the cutoff energy of 76 meV, the modification of carrier kinetic coefficients would be negligible. The virtual absence of phonon confinement effects in a buried GaAs/AlAs structures results from the similarity in elastic constants of GaAs and AlAs, as well as the predominantly transverse nature of the confined modes.

Since a large difference in the elastic properties of the media at an interface is a condition *sine qua non* for strong acoustic-phonon confinement, small *self-supported* structures with (semi)conductor-vacuum interfaces are ideal candidates for the observation of confinement effects. In fact, recent advances in material growth techniques have resulted in the fabrication of free-standing nanostructures[16] and have opened the way to observation of acoustic-phonon confinement effects. Wybourne and co-workers[17] have presented experimental evidence of the two-dimensional nature of

acoustic-phonon modes in self-supported thin films. These experimental findings motivated theoretical investigations by Stroscio and collaborators on the role of acoustic-phonon quantization in free-standing nanostructures.[18–20] Results for phonon spectra and electron-phonon scattering rates in self-supported whiskers,[18,19] dots,[18] and slabs[20] convincingly demonstrate the profound effect of different mechanical boundary conditions on the kinetics of the electron-phonon system.

In summary, buried heterosystems reveal negligible acoustic confinement effects if the materials at the interface possess similar elastic properties (e.g., GaAs/AlAs pair). On the other hand, in self-supported objects confinement effects are strong; however, such structures remain rather exotic and are not easy to integrate into mainstream planar technologies. Yet there exists another configuration that combines the advantages of both buried and free-standing structures: a planar crystal surface.

In this paper we explore the effects of phonon confinement at a crystal-vacuum interface and the interaction of phonons with a near-surface two-dimensional electron gas (2DEG). Such a system supports both extended (reflected) waves and Rayleigh waves that are localized in the vicinity of the surface. The study of the interaction between near-surface quantized electrons and phonons not only is important from a fundamental perspective, but may also lead to the introduction of a different type of channel coupling as well as delay lines into the arsenal of planar nanotechnology. In fact, properties of classical surface acoustic waves (SAW's) are well known and have numerous device applications.[21] Recently, there have been a number of experimental[22] and theoretical[23] studies of the interaction between a classical SAW and 2DEG. Measurements of SAW attenuation were found to be a sensitive probe in the study of the quantum Hall effect.[24]

Our work extends the study of Ezawa *et al.*[25–27] on the electron mobility in silicon metal-oxide-semiconductor field-effect transisters limited by the interaction of electrons with bulk and surface acoustic-phonon modes. These authors used a soft-medium approximation for a SiO_2 layer and assumed a stress-free surface bounding a silicon half space. Ezawa[26] constructed a complete orthonormal set of elastic vibrations supported by the system and quantized them in an ''in-plane phase velocity'' representation. The mobility of electrons occupying six equivalent X valleys was calculated in a quasi-elastic relaxation time approximation. Since the temperature was considered to be in the range 200–300 K, electrons were treated as nondegenerate and an equipartition distribution was taken for the phonon population. Electrons occupied the lowest subband of a triangular potential well located at the Si/SiO_2 interface. Numerical calculations showed that the modification of the phonon modes due to the presence of the boundary can lead to a change of up to 15% in the mobility, depending on the ratio of the two deformation potential constants Ξ_u/Ξ_d.

In this paper we study in detail both mobility and power loss in a 2DEG located in a square or triangular well at a finite distance ℓ from the surface of a GaAs-like semiconductor with a conduction-band minimum at the Γ point. We focus on interaction of electrons with surface and bulk *acoustic* phonons and consider the temperature range where the acoustic-phonon contribution is larger than or comparable to that of optical phonons. Electrons can be assumed to be degenerate for reasonable concentrations of the 2DEG. Since at low temperature the carrier mobility is limited predominantly by static lattice imperfections, we calculate both momentum and *energy* relaxation rates. Kinetic coefficients are calculated within a dielectric formalism[28–32] that fully treats inelasticity of acoustic-phonon scattering and uses the full form of the phonon distribution function.

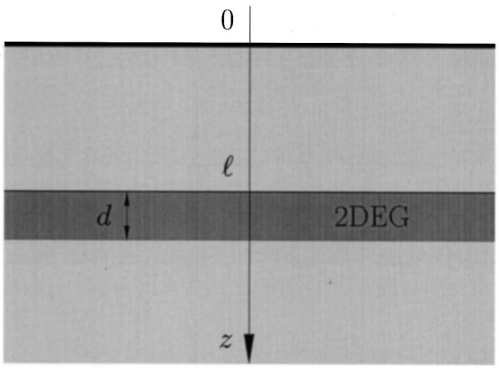

FIG. 1. Two-dimensional electron channel of width d at distance ℓ from the free surface.

This paper is organized as follows. In Sec. II we specify the model system and introduce the relaxation rates to be calculated. Section III presents the general expressions for the energy and momentum relaxation times and contains parameters characterizing the quantized phonon modes and the electron-phonon interaction Hamiltonian. In Sec. IV we make a qualitative, analytical comparison of the electron-phonon interaction in cases of different dimensionalities of electrons and phonons. Section V provides results of numerical calculations and conclusions are formulated in Sec. VI. Auxiliary formulas and expressions can be found in the Appendix.

II. MODEL AND DEFINITIONS

We consider the semiconductor-vacuum system of Fig. 1, where the semiconductor occupies the half space $z>0$. In the isotropic elastic continuum approximation, the material is characterized by longitudinal and bulk sound velocities[33] s_l and s_t and by the lattice dielectric constant ε_0.

Electrons occupy the lowest subband of a square or triangular well at a distance ℓ from the surface. For a *square* quantum well of width d, the density distribution $|\chi(z)|^2$ is nonzero for $\ell<z<\ell+d$, where it is given by

$$|\chi(z)|^2=(2/d)\sin^2\frac{\pi(z-\ell)}{d}. \tag{1a}$$

In a *triangular* well, the electron distribution for $z>\ell$ is taken in the Stern-Howard approximation specified by a variational parameter b:

$$|\chi(z)|^2=(b^3/2)\ (z-\ell)^2e^{-b(z-\ell)}. \tag{1b}$$

Electrons interact with an equilibrium phonon system maintained at a lattice temperature T_0. Due to an applied electric field **E** or to an initial excitation, the electron system

acquires a finite average velocity $\mathbf{u}$ and, in an effective temperature approximation, electron temperature T_e different from the lattice temperature T_0.

Electron–acoustic-phonon scattering causes a change in the average momentum per electron and energy per electron $\langle \mathbf{p} \rangle$ and $\langle \epsilon \rangle$, respectively. For an electron subsystem not far from equilibrium, linearization of collision terms in $\mathbf{u}$ or $T_e - T_0$ facilitates the definition of the *momentum* and *energy* (more precisely, temperature) relaxation times τ_m and τ_ϵ:

$$\left(\frac{\partial \langle \mathbf{p} \rangle}{\partial t} \right)_{\text{coll}} = - \frac{m \mathbf{u}}{\tau_m}, \tag{2}$$

$$\left(\frac{\partial \langle \epsilon \rangle}{\partial t} \right)_{\text{coll}} = - \frac{T_e - T_0}{\tau_\epsilon}, \tag{3}$$

where m is the electron effective mass.

If the electrons are driven out of equilibrium by an applied electric field $\mathbf{E}$, the substitution of collision terms (2) and (3) into the balance equations gives

$$\mathbf{u} = \frac{e \tau_m}{m} \mathbf{E},$$

$$T_e = T_0 + \frac{e^2 \tau_m \tau_\epsilon}{m} E^2.$$

The rest of this paper deals with the calculation of energy and momentum relaxation rates $1/\tau_\epsilon$ and $1/\tau_m$ for a 2DEG interacting with the full set of phonon modes in a semibounded system. Since we are interested in a sufficiently low-temperature range where the acoustic phonon contribution is at least comparable with that of optical phonons, the 2DEG is assumed to be degenerate, i.e.,

$$T \ll F \equiv \hbar^2 k_F^2 / 2m, \tag{4}$$

where $k_F = \sqrt{2 \pi n_2}$ is the Fermi wave vector of a 2DEG and n_2 is an electron sheet density. In addition, we assume that the sound speed is much smaller than the Fermi velocity v_F:

$$s_{l,t} \ll v_F \equiv \hbar k_F / m. \tag{5}$$

III. BASIC EQUATIONS

In Sec. III A we present the general expressions for electron relaxation times; then in Sec. III B we specify the set of phonon modes. Finally, in Sec. III C we introduce the electron-phonon interaction Hamiltonian.

A. Dielectric formalism

We now describe the kinetics of the interacting electron-phonon system within the dielectric formalism[28–32] based on the dielectric functions (polarization operators, noninteracting Green functions, etc.) of the electron and phonon subsystems. The use of the dielectric formalism is equivalent to the Fermi golden rule and the random-phase approximation, but it is particularly convenient for the description of screening and dissipation in an inhomogeneous dielectric medium.

To avoid a cumbersome numerical solution of the Boltzmann kinetic equation for the electron-phonon system, we use a two-parameter shifted equilibrium distribution function for the 2DEG:

$$f_{\mathbf{k}} = f_{T_e} \left[\frac{\hbar^2}{2m} \left(\mathbf{k} - \frac{m}{\hbar} \mathbf{u} \right)^2 \right], \tag{6}$$

where $f_T(\epsilon) \equiv \{1 + \exp[(\epsilon - \mu)/T]\}^{-1}$ is the Fermi-Dirac distribution. Unlike the relaxation time approximation, such a model accounts well for the inelasticity in scattering and becomes exact in the limit of strong electron-electron interaction.[35]

The inverse momentum and energy relaxation times, defined by Eqs. (2) and (3), can be expressed in terms of integrals over the transferred momentum $\hbar q$ and the energy $\hbar \omega$ as[29]

$$\left. \begin{matrix} 1/\tau_m \\ 1/\tau_\epsilon \end{matrix} \right\} = \frac{1}{\pi^2 n_2} \int_0^\infty \frac{d\omega}{\omega^2} \int_0^\infty q^3 \, dq \left\{ \begin{matrix} T/2m \\ \omega^2/q^2 \end{matrix} \right\} \times \frac{\text{Im } \pi_{\text{ph}}(\omega,q) \, \text{Im } \pi_e(\omega,q)}{|1 + \Delta \varepsilon_e(\omega,q)/\varepsilon_s(\omega,q)|^2} \left[\frac{\hbar \omega / 2T}{\sinh(\hbar \omega / 2T)} \right]^2. \tag{7}$$

Here the dielectric function of the 2DEG, $\Delta \varepsilon_e$, is related to its polarization function π_e,

$$\pi_e(\omega, \mathbf{q}) = \frac{2}{\mathcal{S}} \sum_{\mathbf{k}} \frac{f_{\mathbf{k}+\mathbf{q}} - f_{\mathbf{k}}}{\hbar \omega - \epsilon_{\mathbf{k}+\mathbf{q}} + \epsilon_{\mathbf{k}} + i0}, \tag{8}$$

as

$$\Delta \varepsilon_e(\omega,q) = v_{\text{Coul}}(q) \, \pi_e(\omega,q), \tag{9}$$

where $\mathcal{S}$ is the area of the system and $v_{\text{Coul}}(q)$ is the Fourier transform of the two-dimensional (2D) Coulomb potential

$$v_{\text{Coul}}(q) = 2 \pi e^2 / q. \tag{10}$$

The explicit expression for the polarization function of the degenerate 2DEG is provided in Appendix A.

The total polarization function of the system in the absence of electrons

$$\pi_s(\omega,q) = v_{\text{Coul}}(q) / \varepsilon_s(\omega,q) \tag{11}$$

and its phonon part π_{ph} are obtained by weighting the linear-response functions with the electron density functions:

$$\pi_{s,\text{ph}}(\omega,q) = \int dz |\chi(z)|^2 \times \int dz' |\chi(z')|^2 \pi_{s,\,\text{ph}}(\omega,q,z,z'). \tag{12}$$

Here the linear-response functions $\pi(\omega,q,z,z')$ specify the Fourier component of the potential $V(z)$ induced by the electron distribution $\rho(z')$,

$$\hat{V}(\omega,q,z) = \int dz' \, \pi(\omega,q,z,z') \hat{\rho}(\omega,q,z'). \tag{13}$$

Explicit formulas for functions $\varepsilon_s(\omega,q)$ and $\pi_{\rm ph}(\omega,q)$ are derived in Appendix B and Sec. III C from Eq. (13).

B. Phonon modes

The free phonon modes in an elastic medium can be characterized by the set of quantum numbers $J=(\mathbf{q},\Omega,j)$, where $\mathbf{q}=(q_x,q_y)$ is an in-plane wave vector, Ω is the phonon frequency,[36] and $j=H,L,T,R$ specifies the different types of elastic modes as discussed below. In the second quantization representation, the phonon displacement operator takes the form

$$\hat{\mathbf{U}}(\mathbf{r},z,t)=\sum_J \sqrt{\frac{\hbar}{2\rho\Omega}}\,[\mathbf{u}_J(\mathbf{r},z)\,\hat{b}_J e^{-\omega t}+\text{ H.c.}], \quad (14)$$

where $\mathbf{r}=(x,y)$ and $\hat{b}$ is a phonon annihilation operator at time $t=0$. The classical acoustic wave displacements $\mathbf{u}$ are taken as plane waves in the x,y directions,

$$\mathbf{u}_J(\mathbf{r},z)=\mathbf{u}_J(z)\,\frac{e^{i\mathbf{q}\cdot r}}{\sqrt{\mathcal{S}}} \quad (15)$$

and must obey the orthonormality conditions

$$\int dz\ \mathbf{u}^{(\alpha)}_{j\Omega\mathbf{q}}(z)\ \mathbf{u}^{(\alpha')*}_{j'\Omega'\mathbf{q}}(z)=\delta_{\alpha,\alpha'}\delta_{j,j'}\delta(\Omega-\Omega').$$

Here $\alpha=x,y$ or z. Dirac's delta function is replaced by the Kronecker function $\delta(\Omega-\Omega')\to\delta_{\Omega,\Omega'}$ if either Ω or Ω' belongs to the discrete part of spectrum.

The classical displacement vectors $\mathbf{u}$ and the wave spectrum are found from the solution of the elastic wave equation with the stress-free boundary condition $\sigma_{\alpha z}=0$ imposed on the strain tensor σ at $z=0$.[4] Such a solution can be obtained as a linear combination of bulk plane waves $\exp(\pm ik_l z)$ and $\exp(\pm ik_t z)$, where k_l and k_t correspond to the normal components of bulk longitudinal and transverse waves with in-plane wave vector, $\mathbf{q}$ and frequency Ω:

$$k_{l,t}=\sqrt{(\Omega/s_{l,t})^2-q^2}. \quad (16)$$

In isotropic media, we can direct the wave vector $\mathbf{q}$ along the x axis. Then the displacement in the y direction is decoupled from the other components, defining the *horizontal shear* mode ($j\equiv H$) with

$$u_x^{(H)}=u_z^{(H)}=0\,,\quad u_y^{(H)}(z)=\sqrt{\frac{2\Omega}{\pi s_t^2 k_t}}\cos(k_t z), \quad (17)$$

and frequency $\Omega>s_t q$. These purely transverse modes do not contribute to the deformation potential coupling considered in our subsequent analysis.

To describe the remaining elastic modes, it is convenient to introduce the scalar potentials ϕ and ψ. In the case where $\mathbf{q}\|\mathbf{x}$, the displacement vector components can be written as

$$\mathbf{u}(\mathbf{r},z)=\nabla\phi+\nabla\times[\psi(\mathbf{r},z)\cdot\mathbf{e}_y], \quad (18)$$

where ϕ and ψ satisfy wave equations with propagation speeds s_l and s_t, respectively. One can also define components $\phi(z)$ and $\psi(z)$ in a way similar to Eq. (15):

$$\left.\begin{matrix}\phi_J(\mathbf{r},z)\\ \psi_J(\mathbf{r},z)\end{matrix}\right\}=\left\{\begin{matrix}\phi_J(z)\\ \psi_J(z)\end{matrix}\right\}\frac{e^{i\mathbf{q}\cdot\mathbf{r}}}{\sqrt{\mathcal{S}}}. \quad (19)$$

The rest of this subsection specifies the remaining three acoustic modes: incident longitudinal ($j\equiv L$), incident transverse ($j\equiv T$), and Rayleigh ($j\equiv R$) waves.[36] Note that even a pure longitudinal or transverse wave acquires a mixed character after reflection from the surface.

1. Incident longitudinal wave

The incident longitudinal wave ($j\equiv L$) exists over a continuous range of frequencies $\Omega>s_l q$ and is specified by the scalar potentials

$$\phi^{(L)}_{q\Omega}(z)=\frac{1}{\sqrt{2\pi\Omega k_l}}[e^{-ik_l z}-A\ e^{ik_l z}],$$

$$\psi^{(L)}_{q\Omega}(z)=-\frac{B}{\sqrt{2\pi\Omega k_t}}\ e^{ik_t z}. \quad (20)$$

Here

$$A(\lambda,\tau)=\frac{(\tau^2-1)^2-4\lambda\tau}{(\tau^2-1)^2+4\lambda\tau} \quad (21)$$

and

$$B(\lambda,\tau)=\frac{4\sqrt{\lambda\tau}(\tau^2-1)}{(\tau^2-1)^2+4\lambda\tau}, \quad (22)$$

where $\lambda\equiv k_l/q$ and $\tau\equiv k_t/q$; furthermore, $A^2+B^2=1$.

2. Incident transverse wave

This type of wave exists for frequencies in the range $\Omega>s_t q$ and is given by

$$\phi^{(T)}_{q\Omega}(z)=\frac{B}{\sqrt{2\pi\Omega k_l}}\ e^{ik_l z}, \quad (23)$$

$$\psi^{(T)}_{q\Omega}(z)=\frac{1}{\sqrt{2\pi\Omega k_t}}[e^{-ik_t z}-A\ e^{ik_t z}].$$

In the subinterval of $s_l q>\Omega>s_t q$ the longitudinal component of the wave becomes evanescent and analytical continuation $k_l=i|k_l|$ is used.

3. Rayleigh wave

The Rayleigh wave is localized in the vicinity of the surface and possesses a discrete (at fixed q) frequency $\Omega=s_R q$. The surface wave velocity s_R can be obtained from the equation[4]

$$(\tau^2-1)^2+4\lambda\tau=0. \quad (24)$$

Both the longitudinal and transverse components of the displacement vectors are evanescent in the z direction and the continuations $k_l\to i|k_l|$ and $k_t\to i|k_t|$ should be employed. The scalar potentials are given by

$$\phi^{(R)}_{q\Omega_R} = \sqrt{\frac{R}{q}}\ e^{-|k_l|z}, \tag{25}$$

$$\psi^{(R)}_{q\Omega_R} = \sqrt{\frac{R}{q}}\ \frac{-2i|\lambda|}{1+|\tau|^2}\ e^{-|k_t|z},$$

where the constant,

$$R = 2|\lambda|\,|\tau|^2/(|\lambda|-|\tau|)(|\lambda|-|\tau|+2|\lambda|\,|\tau|^2) \tag{26}$$

depends only on the Poisson ratio of the material. Since the characteristic equation (24) also specifies the poles of functions A and B in Eqs. (21) and (22), the constant R is proportional to the residue in the complex Ω plane

$$R = \text{Res}\ \left.\frac{A(\lambda,\tau)}{i\lambda}\right|_{\Omega=s_R q}. \tag{27}$$

C. Electron-phonon coupling

In this subsection we derive the dissipative part of the phonon polarization function π_{ph} defined by Eq. (13). We start from the electron-phonon interaction Hamiltonian in the Heisenberg form

$$\hat{\mathcal{H}}_{e\text{-ph}}(t) = \sum_{\mathbf{q},\mathbf{k}}\ \hat{a}^{\dagger}_{\mathbf{k}+\mathbf{q}}(t)\hat{a}_{\mathbf{k}}(t)\ \hat{V}_{\mathbf{q}}(t), \tag{28}$$

where $\hat{a}$ ($\hat{a}^{\dagger}$) is the electron annihilation (creation) operator.

In this paper we consider the deformation potential interaction specified by a constant Ξ:

$$\hat{V}(\mathbf{r},z,t) = \Xi\ \ \text{div}\ \hat{\mathbf{U}}(\mathbf{r},z,t). \tag{29}$$

Taking the phonon displacement operator $\hat{\mathbf{U}}$ to be Eq. (14) and using the identity $\nabla^2\phi = \ddot{\phi}/s_l^2 = -(\omega^2/s_l^2)\ \phi$, we find the interaction operator

$$\hat{V}(\mathbf{r},z,t) = -\ \Xi\ \sum_J\ \frac{\Omega^2}{s_l^2}\sqrt{\frac{\hbar}{2\rho\Omega\mathcal{S}}} \times[\hat{b}_J\phi_{J\mathbf{q}}(\mathbf{z})\ \ \mathbf{e}^{i(\mathbf{q}\cdot\mathbf{r}-\Omega t)} + \text{H.c.}]. \tag{30}$$

According to the Kubo theorem,[37] the dissipative part of the linear-response function π_{ph} is proportional to the antisymmetric part of correlation of the potentials $\hat{\mathbf{V}}$:

$$\text{Im}\ \pi(\omega,\mathbf{q},z,z') = \frac{1}{2\hbar}\ \int_{-\infty}^{\infty} dt\ \int d^2r e^{i(\omega t-\mathbf{q}\cdot\mathbf{r})}\langle \hat{V}(t,\mathbf{r},z) \times \hat{V}(0,\mathbf{0},z') - \hat{V}(0,\mathbf{0},z')\hat{V}(t,\mathbf{r},z)\rangle. \tag{31}$$

Substituting expression (30) into Eq. (31) and performing the necessary commutations, we find

$$\text{Im}\ \pi_{\text{ph}}(\omega,q,z,z') = \frac{\pi\Xi^2\Omega^3}{2\rho s_l^4}\ \sum_{j,\Omega}\ \phi_{jq\Omega}(z)\phi^{*}_{jq\Omega}(z') \times[\delta(\omega-\Omega)-\delta(\omega+\Omega)]. \tag{32}$$

We found a general expression for the polarization function of phonons coupled to electrons by the deformation potential in a system, which is inhomogeneous in the z direction. Using the scalar phonon potentials ϕ in Eqs. (20), (23), and (25), we obtain π_{ph} for phonons in a half space:

$$\text{Im}\ \pi_{\text{ph}}(\omega,\mathbf{q},z,z') = \frac{\Xi^2}{2\rho s_l^4}\ \frac{\omega^2}{q}\ \times\begin{cases} \dfrac{1}{\lambda}\cos\lambda q(z-z') - \dfrac{A(\lambda,\tau)}{\lambda}\cos\lambda q(z+z') & \text{at}\ \ \omega > s_l q \\ \dfrac{|B(i|\lambda|,\tau)|^2}{2|\lambda|}\ e^{-|\lambda|q(z+z')} & \text{at}\ \ s_l q > \omega > s_t q \\ \dfrac{\pi}{K(\sigma)}\ e^{-|\lambda|q(z+z')}\omega\ \delta(\omega-s_R q) & \text{at}\ \ \omega \approx s_R q. \end{cases} \tag{33}$$

For comparison, we present the polarization function of acoustic phonons in an unbounded medium

$$\text{Im}\ \pi_{\text{bulk}}(\omega,\mathbf{q},z,z') = \frac{\Xi^2}{2\rho s_l^4}\ \frac{\omega^2}{\lambda q}\cos\lambda q(z-z')\quad \text{at}\ \omega > s_l q. \tag{34}$$

Examination of Eqs. (33) and (34) shows that the phonon polarization function in a half space is equal to the sum of the bulk part depending on $|z-z'|$ and the image part depending on $z+z'$.

Finally, we weight the function $\pi_{\text{ph}}(\omega,\mathbf{q},z,z')$ with the electron density function $|\chi(z)|^2$. Substituting Eq. (33) into Eq. (12) and using the definitions of form factors Z and $\mathcal{Z}$ in Appendix C, we obtain

$$\text{Im}\ \pi_{\text{ph}}(\omega,q) = \text{Im}\ \pi_{\text{bulk}}(\omega,q) + \text{Im}\ \pi_{\text{bulk corr}}(\omega,q) + \text{Im}\ \pi_{\text{tot refl}}(\omega,q) + \text{Im}\ \pi_{\text{Rayleigh}}(\omega,q). \tag{35}$$

Here the first term in Eq. (35) coincides with the contribution of the *bulk* phonons

$$\text{Im}\ \pi_{\text{bulk}}(\omega,q) = \frac{\Xi^2}{2\rho s_l^4}\ \frac{\omega^2}{\lambda q}\ \ \mathcal{Z}_{\text{bulk}}(\lambda q)\quad \theta(\omega-s_l q). \tag{36}$$

The image part of the polarization function accounts for modifications due to the free boundary at $z=0$ and is given by the sum of the expressions (θ is a step function)

$$\mathrm{Im}\ \pi_{\mathrm{bulk\ corr}}(\omega,q)=-\frac{\Xi^2}{2\rho s_l^4}\ \frac{\omega^2}{q}\ \frac{A(\lambda,\tau)}{\lambda}\ \mathcal{Z}_{\mathrm{image}}(\lambda q)\times\theta(\omega-s_l q), \tag{37}$$

$$\mathrm{Im}\ \pi_{\mathrm{tot\ refl}}(\omega,q)=\frac{\Xi^2}{2\rho s_l^4}\ \frac{\omega^2}{q}\ \frac{|B(i|\lambda|,\tau)|^2}{2|\lambda|}\times Z_{\mathrm{image}}(|\lambda|q)\,\theta(s_l q-\omega)\,\theta(\omega-s_t q), \tag{38}$$

$$\mathrm{Im}\ \pi_{\mathrm{Rayleigh}}(\omega,q)=\frac{\Xi^2}{2\rho s_l^4}\ \frac{\omega^2}{q}\ \pi R Z_{\mathrm{image}}(|\lambda|q)\times\omega\,\delta(\omega-s_R q). \tag{39}$$

Equations (37)–(39) may be identified with (i) corrections to the bulk phonon modes due to the presence of the surface and contributions of (ii) totally reflected modes as well as (iii) Rayleigh phonons.

IV. QUALITATIVE ANALYSIS

It is possible to provide analytical order-of-magnitude estimates of the relaxation rates in Eq. (7) in order to obtain the dependence of the scattering rates on temperature, electron concentration, and other parameters of the problem. To gain an understanding of the effects of phonon quantization on the relaxation of the 2DEG, we consider both the case of (a) unmodified, bulk phonons [see Eq. (36)] and (b) the complete phonon set as given by Eqs. (35)–(39); we will also compare these estimates with the results for interacting (c) bulk electrons and bulk phonons (cf. Appendix D).

We note that the integrands of Eqs. (7) and (D1) increase monotonically with the transferred momentum q and energy ω until the correspondent cutoff values are reached. This leads to the following estimates for the relaxation rates valid for arbitrary degeneracy of the electron system:

$$\left.\begin{matrix}1/\tau_m\\ 1/\tau_\epsilon\end{matrix}\right\}\sim\frac{q_{\max}^{\nu+1}}{\overline{\epsilon}\,\overline{v}}\ \mathrm{Im}\ \pi_{\mathrm{ph}}(\omega_{\max},q_{\max})\ \begin{cases}T/m\\ \omega_{\max}^2/q_{\max}^2.\end{cases} \tag{40}$$

Here $\nu=2,3$ specifies the dimensionality of the electron system (in fact, this result applies to one-dimensional electrons $\nu=1$). The electron mean kinetic energy and the velocity are given by either their Fermi or thermal values: $\overline{\epsilon}\sim\max(F,T)$ and $\overline{v}\equiv\sqrt{2\,\overline{\epsilon}/m}\sim\max(v_F,v_T)$.

The maximum momentum and energy transferred during a single electron-phonon collision are determined as a result of the competition between several mechanisms:

$$q_{\max}\sim\min(2\,\overline{k},\omega_{\max}/s), \tag{41}$$

$$\omega_{\max}\sim\min(T/\hbar,q_{\max}\overline{v}). \tag{42}$$

Here the conditions $q\lesssim 2\,\overline{k}\equiv 2\min(k_F,k_T)$ and $\omega\lesssim q\,\overline{v}$ are due to the factor $\mathrm{Im}\ \pi_e(\omega,q)$ in the expressions for the relaxation times; see also Eqs. (A1) and (A2). The former inequality limits the momentum transfer to the effective diameter of the electron distribution function, while the latter is a result of the momentum and energy conservation laws.[38] Similarly, the condition $\omega\lesssim T/\hbar$ stems from the factor $[(\hbar\omega/2T)/\sinh(\hbar\omega/2T)]^2$ in Eqs. (7) and (D1) and, for degenerate electrons, limits the energy transfer to a narrow region of width T near the Fermi surface. Finally, the condition $q_{\max}<\omega_{\max}/s$ implies that only the electrons with a phase velocity exceeding the speed of sound may interact with the phonons (Cherenkov effect).

Spatial confinement of the electron system leads to two additional cutoffs for q and ω. Prior to the introduction of these conditions we note that for electrons to occupy the lowest quantization subband, the following inequality must be obeyed:

$$k_F\lesssim 1/d, \tag{43}$$

where d is the effective transverse width of electron channel and the relation $k_F\sim 1/d$ corresponds to the maximum occupancy of the lowest subband.

Electron confinement in the z direction breaks the momentum conservation law for q_z, replacing it by a weaker inequality $q_z\lesssim 1/d$. Taking into account the relation $\omega\sim s\sqrt{q^2+q_z^2}$ and Eq. (43), we find a condition augmenting Eq. (42) for a spatially confined electron system:

$$\omega\lesssim s/d. \tag{44}$$

Finally, the surface corrections to the phonon spectrum weaken with the increasing distance ℓ between the surface and the 2DEG. The following inequality arises from the form factors Z_{image} in Eqs. (37)–(39):

$$q\lesssim 1/\ell. \tag{45}$$

Note that Eq. (45) does not apply to the partial contribution of the bulk phonon modes in Eq. (36).

As shown below, the temperature and concentration dependence of the relaxation frequencies depend critically on the competition of the two cutoffs $q\lesssim\overline{k}$ and $q\lesssim\omega/s$. These two conditions become equivalent at $T\sim T_{\mathrm{cr}}$, where the critical temperature is defined as

$$T_{\mathrm{cr}}\sim\hbar s\,\overline{k}\sim\sqrt{ms^2\,\overline{\epsilon}}. \tag{46}$$

Since at temperatures of the order of or below T_{cr} the electron gas is usually degenerate, Eq. (46) may be reduced to $T_{\mathrm{cr}}\sim\hbar s k_F$. In view of Eq. (43), we find

$$T_{\mathrm{cr}}\lesssim\hbar s/d, \tag{47}$$

where the equality $T_{\mathrm{cr}}\sim\hbar s/\ell$ is reached when the lowest quantization subband is practically filled.

To analyze the temperature dependence of the relaxation rates for different dimensionalities of electrons and phonons, we present schematically in Figs. 2 and 3 the regions of transferred momentum and energy contributing to Eqs. (7) and (D1) at small ℓ. Due to the monotonically increasing

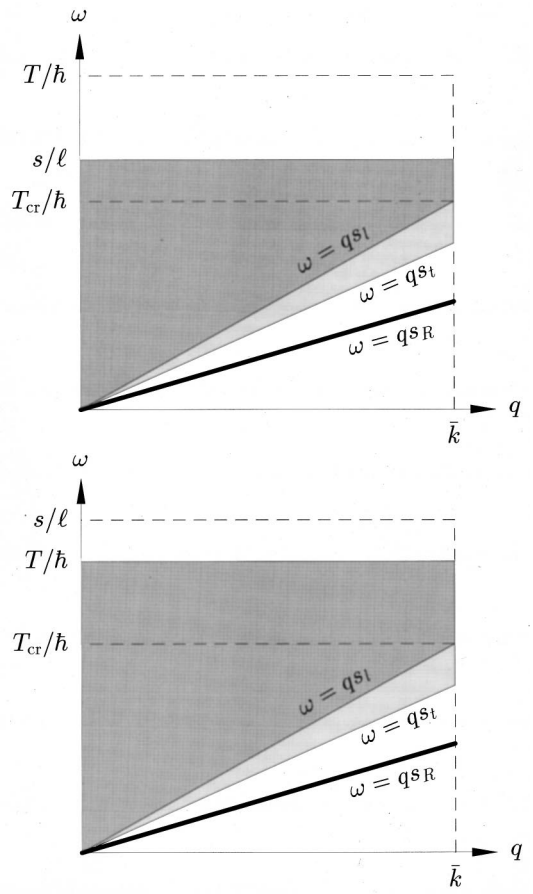

FIG. 2. Regions of transferred momentum q and frequency ω for $T>\hbar s/d>T_{cr}$ (upper panel) and $\hbar s/d>T>T_{cr}$ (lower panel).

integrands, the dominant contributions are given by the maximum possible values of ω and q.

Scattering of the 2DEG with bulk and bulklike phonons contributes to the dark shaded region at $\omega>s_l q$. The totally reflected phonon modes are shown by the light shading at $s_l q>\omega>s_t q$ and the two-dimensional Rayleigh phonons correspond to the thick line at $\omega=s_R q$. In contrast, the interaction of *bulk electrons* and phonons occurs at $\omega=s_l q<\min(T/\hbar,T_{\rm cr}/\hbar)$, as specified by the factor $\delta(\omega-s_l q)$ in Eq. (D3), where the bulk wave vector $\mathbf{q}=(q_x,q_y,q_z)$. Below we analyze the relaxation rates in the limits of high and low temperature $T\gtrsim T_{\rm cr}$ and $T\lesssim T_{\rm cr}$.

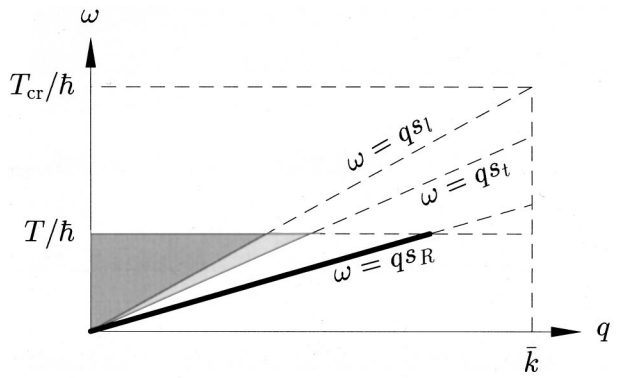

FIG. 3. Regions of transferred momentum q and frequency ω in a low-temperature limit $T<T_{\rm cr}$.

A. High-temperature regime ($T>T_{\rm cr}$)

For interacting *bulk electrons* and phonons, the effective transferred momentum and energy are given by $q_{\max}=\omega_{\max}/s_l\sim 2\overline{k}$. From Eqs. (40) and (D3) we find

$$\left.\begin{matrix}1/\tau_m\\1/\tau_\epsilon\end{matrix}\right\}\sim\frac{\Xi^2}{\rho s^2}\frac{m^{3/2}}{\hbar^4 S_3(\overline{k})}\quad\overline{\epsilon}^{1/2}\begin{cases}T\\ms^2,\end{cases}\tag{48}$$

where the three-dimensional screening factor is given by $S_3(q)\sim[1+4\pi^2e^2n_3/\varepsilon_0\overline{\epsilon q}^2]^2$.

As seen from Eq. (48), the ratio of the energy and momentum relaxation rates is equal to $T/ms^2\ll 1$; i.e., the phonon scattering is quasielastic. In the nondegenerate case where $\overline{\epsilon}\sim T$, the standard results $1/\tau_m\propto T^{3/2}$ and $1/\tau_\epsilon\propto T$ are reproduced.[35] For degenerate electrons, $1/\tau_m\propto T$ and the energy relaxation rate $1/\tau_\epsilon$ depends weakly on the temperature.

For a *2D electron channel*, the principal contribution is given by bulklike phonons with $q\sim 2\overline{k}$ since they contribute to the maximum energy transfer ω for the same $q_{\max}\sim\overline{k}$. Depending on the relation between T and $\hbar s/d$, two situations are possible.

In the case when $T>\hbar s/d\gtrsim T_{\rm cr}$ (Fig. 2, upper panel), we substitute the cutoff values $q_{\max}\sim\overline{k}$ and $\omega_{\max}\sim s/d$ into Eq. (40) and obtain

$$\left.\begin{matrix}1/\tau_m\\1/\tau_\epsilon\end{matrix}\right\}\sim\frac{\Xi^2}{\rho s^2}\frac{m}{\hbar^3 S_2(\overline{k})}\quad\frac{1}{d}\begin{cases}T\\ \hbar^2 s^2/\overline{\epsilon}d^2,\end{cases}\tag{49}$$

where the factor $S_2(q)\sim[1+2\pi e^2 n_2/\varepsilon_0\overline{\epsilon q}]^2$ accounts for screening by the 2DEG. In a typical situation of an almost completely filled lowest subband $\overline{k}d\sim 1$, expression (49) coincides with its bulk value in Eq. (48).

The opposite case of $\hbar s/d>T>T_{\rm cr}$ (see Fig. 2, lower panel) can be realized only for a weakly populated lowest subband [cf. Eq. (47)] and occurs rarely in practice. Substituting $q_{\max}\sim\overline{k}$ and $\omega_{\max}\sim T/\hbar$ into Eq. (40), we find

$$\left.\begin{matrix}1/\tau_m\\1/\tau_\epsilon\end{matrix}\right\}\sim\frac{\Xi^2}{\rho s^2}\frac{m}{\hbar^4 s S_2(\overline{k})}\quad\frac{T^2}{\overline{\epsilon}}\begin{cases}\overline{\epsilon}\\ T.\end{cases}\tag{50}$$

In this regime, phonon scattering is strongly inelastic: $\tau_\epsilon\sim\tau_m$ for nondegenerate electrons and $\tau_\epsilon\gg\tau_m$ for degenerate statistics (i.e., effective temperature relaxation is faster than the momentum relaxation). Thus the frequently used quasielastic approximation in the energy conservation law[39] is invalid for this regime.[40]

B. Bloch-Grüneisen regime ($T<T_{\rm cr}$)

For $T<T_{\rm cr}$, the momentum and energy transfer cutoffs are given by $q_{\max}\sim\overline{k}$ and $\omega_{\max}\sim T/\hbar$, respectively, as shown in Fig. 3. From Eq. (40) we obtain the following estimate which is valid for any dimensionality of electrons ($\nu=2,3$) and phonons:

$$\left.\begin{matrix}1/\tau_m\\1/\tau_\epsilon\end{matrix}\right\}\sim\frac{\Xi^2}{\rho s^2}\frac{T^4}{\hbar^4\sqrt{m\overline{\epsilon}}\,s^4\,S_\nu(\overline{k})}\quad\begin{cases}T\\ms^2.\end{cases}\tag{51}$$

As seen from Fig. 3, the Rayleigh phonons contribute to maximum energy transfer $\hbar\omega$ as a result of the lower propagation speed ($s_R < s_t < s_l$). Therefore, despite a similar temperature dependence of all phonon modes, the Rayleigh phonon contribution to relaxation may become dominant for $T \ll T_{\rm cr}$. Rayleigh modes make a large contribution only when there is a small separation between the 2DEG and the surface ($\ell < 1/\overline{k}$); in the limit of large ℓ, the surface contributions vanish.

In this study we have not considered piezoelectric phonon scattering, which prevails for sufficiently low temperatures.[35,41] However, the details of the electron-phonon coupling do not affect our kinematic analysis as shown in Figs. 2 and 3.

V. NUMERICAL RESULTS AND DISCUSSION

In our numerical calculations we neglect the difference in the elastic properties of the quantum well and barrier materials and use the following parameter set for GaAs:[42] crystal density $\rho = 5.32$ g/cm^3, lattice dielectric constant $\varepsilon_0 = 12.5$, electron effective mass $m = 0.067 m_0$, and deformation potential constant $\Xi = 8.0$ eV. Based on the components of the elastic stiffness matrix, $C_{11} = 11.88 \times 10^{11}$ dyn/cm^2, $C_{12} = 5.38 \times 10^{11}$ dyn/cm^2, and $C_{44} = 5.94 \times 10^{11}$ dyn/cm^2, we find in the isotropic approximation[33] that the propagation speeds are $s_l = 5.14 \times 10^5$ cm/s for longitudinal waves, $s_t = 3.02 \times 10^5$ cm/s for transverse waves, and $s_R = 2.77 \times 10^5$ cm/s for Rayleigh waves.

In Fig. 4 we show the dependence of the momentum and energy relaxation rates, calculated from Eq. (7), versus the lattice temperature T for a square quantum well of width $d = 50$ Å located at the crystal surface. A carrier concentration of $n = 10^{12}$ cm^{-2} corresponds to the case of degenerate electron statistics for the temperature range under consideration. The thin solid lines corresponds to bulk phonons that are not modified due to the presence of the free surface. The thick solid lines represent the total rates of electron relaxation due to the complete set of near-surface phonon modes; these contributions are designated as follows: bulklike (dotted line), Rayleigh (dashed line), and totally reflected waves (dash-dotted line). At temperatures below 2 K the piezoelectric scattering mechanism becomes dominant;[41] however, the low-temperature range of Fig. 4 is depicted in order to demonstrate the asymptotic temperature dependences of the deformation potential scattering rates.

In agreement with the qualitative analysis of Sec. IV, all partial contributions to the total scattering rates, as well as the rates due to the unmodified bulk phonons, have the same temperature dependence in the limits of $T \gg T_{\rm cr}$ and $T \ll T_{\rm cr}$. Namely, in the high-temperature limit the momentum relaxation rates satisfy $1/\tau_m \propto T$, while the energy relaxation rates saturate to a constant value; see Eq. (49). In the Bloch-Grüneisen regime, the dependences $1/\tau_m \propto T^5$ and $1/\tau_m \propto T^4$ are observed, in agreement with the Eq. (51).

Although the strengths of electron coupling to different phonon modes have the same overall temperature behavior, their relative contributions to the relaxation rates depend on the temperature interval considered. For high temperature, the surface phonon contribution is more than an order of magnitude weaker than that of bulklike modes and 10% of

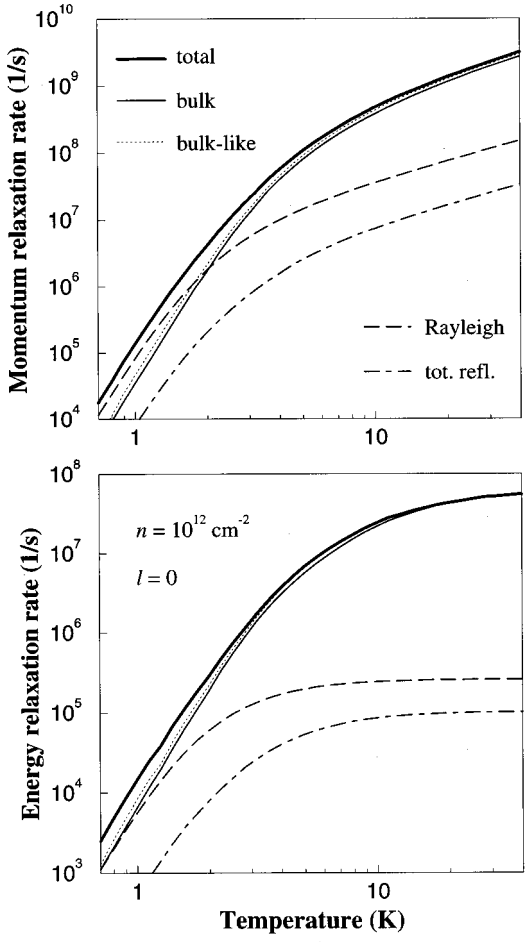

FIG. 4. Momentum (upper panel) and energy (lower panel) relaxation rates of a 2DEG vs temperature. Electrons with a concentration $n = 10^{12}$ cm^{-2} occupy a square quantum well of width $d = 50$ Å located at the surface $\ell = 0$.

the change in the scattering rates is due to the modification of bulk modes near the surface. In contrast, in the Bloch-Grüneisen regime, the partial contribution of the surface Rayleigh waves increases and may even exceed the contribution of the bulklike waves. As explained in Sec. IV, the interaction with Rayleigh phonons is enhanced due to their lower propagation speed and therefore larger assisted momentum transfer; see the thick line in Fig. 3. Finally, the contribution of the totally reflected modes to deformation potential scattering is negligible for all temperatures because of their predominantly transverse character, i.e., $B \ll 1$ in Eq. (23).

The dependence of the relaxation rates on the distance ℓ between the electron channel and the semiconductor surface is presented in Figs. 5 and 6. The partial contributions of different phonon modes are shown in Fig. 5 for a temperature $T = 2$ K. As one can see, the contributions of the surface (dashed line) and totally reflected (dash-dotted line) modes decrease rapidly with distance ℓ from the surface due to the factor $\exp(-2q\ell)$ in Eq. (C3) for the form factor $Z_{\rm image}(q)$. The well-pronounced oscillatory behavior of the total scattering rates (thick solid line) is due primarily to the surface corrections to the bulk phonon modes [cf. the term with $\cos \lambda q(z+z')$ in Eq. (33) for the phonon polarization func-

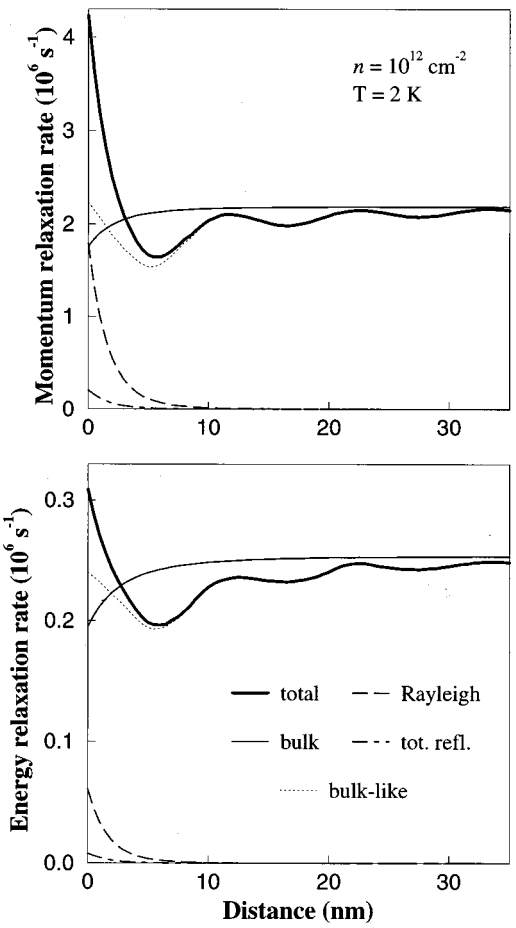

FIG. 5. Momentum (upper panel) and energy (lower panel) relaxation rates of a 2DEG vs. distance ℓ. Electrons with a concentration $n=10^{12}$ cm^{-2} occupy a square quantum well of width $d=50$ Å. The temperature T is 2 K.

tion]. With increasing distance ℓ, the amplitude of oscillations decreases and the scattering rates approach their bulk limit. Finally, we notice that the dip in the scattering rates for unmodified bulk phonons (thin solid line) is caused by a decrease of the effective system dielectric function in Eq. (B2), from $\varepsilon_s(q)\sim\varepsilon_0$ at large ℓ to $(\varepsilon_0+1)/2$ at $\ell=0$. The small value of $\varepsilon_s(q)$ leads to an enhanced contribution of electrons to the screening factor $|1+\Delta\varepsilon_e(\omega,q)/\varepsilon_s(\omega,q)|^{-2}$ in Eq. (7) and therefore to a decrease in the scattering rates for small ℓ.

In Fig. 6 we present the distance dependence of the momentum relaxation rate $1/\tau_m$ for different forms of the electron confining potential ($T=4.2$ K). The dashed (dotted) line corresponds to a square quantum well of width $d=100$ Å (30 Å). The relaxation rates for electrons in a triangular well of effective width[43] $6/b=50$Å (solid line) are close to those for electrons in a square quantum well of width $d=50$ Å (not shown).

As seen from Fig. 6, a change in the well width does not change the period of oscillations, but shifts their phase. This is consistent with the following dependence of the surface corrections to the phonon polarization function in Eq. (37): Im $\pi_{\text{bulk corr}}(\omega,q)\propto\mathcal{Z}_{\text{image}}(q)\propto\cos q(2\ell+d)$. Since, in the Bloch-Grüneisen regime, the effective momentum transfer is

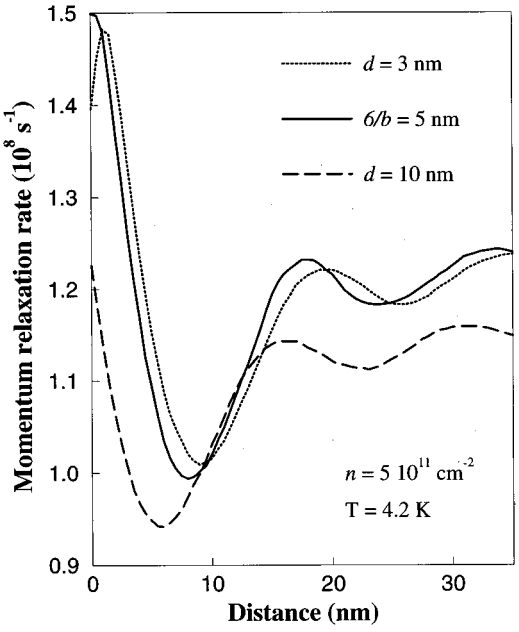

FIG. 6. Momentum relaxation rate $1/\tau_m$ vs distance ℓ. Solid line, triangular quantum well with effective width $6/b=50$ Å; dashed (dotted) line, square quantum well of width $d=100$ Å ($d=30$ Å). The electron concentration $n=5\times10^{11}$ cm^{-2}; temperature $T=4.2$ K.

$q\sim T/\hbar s_l$ (cf. Fig. 3), the period of oscillations can be estimated as $L\sim\pi/q\sim\pi\hbar s_l/T$, which is consistent with the value $L\sim20$ nm from Fig. 3.

VI. CONCLUSIONS

In this paper we have reported our studies on the interaction of a near-surface channel of 2D electrons with the complete set of acoustic-phonon modes supported by a semibound semiconductor structure. Using the dielectric formalism, we have calculated both the momentum and energy relaxation rates of a 2DEG and analyzed the relative contributions of bulklike and surface phonon modes for GaAs material.

At high temperatures, the surface phonon contribution is small and the modification of bulklike phonons leads to approximately a 10% change in mobility. In the low-temperature regime, the electron relaxation rates exhibit pronounced oscillations with respect to the position of the electron channel, providing the possibility of tailoring carrier-phonon interactions in nanostructures to minimize dissipation.

The most significant result of this work is the strong interaction of electrons with Rayleigh phonons in the Bloch-Grüneisen regime. While the momentum and the energy transferred to the *bulklike* phonons are radiated to the bulk of crystal and lost, the emitted *surface* phonons remain in the channel and continue to influence electron kinetics. The relatively weak attenuation of two-dimensional Rayleigh phonons facilitates their use for coupling between different electron channels and their constant speed facilitates the de-

sign of built-in delay lines. Thus the study of surface effects on the carrier-phonon interaction is important for the design of semiconductor nanostructures within existing planar technologies.

ACKNOWLEDGMENTS

This work was supported by the U.S. Army Research Office and the Office of Naval Research.

APPENDIX A: ELECTRON POLARIZATION

For the strongly degenerate case $F=\pi^2\hbar^2 n_2/m \gg T$ and in the limit of $\hbar\omega \lesssim T$ [see the factor in the square brackets in Eq. (7)], the polarization function of the 2DEG given by Eq. (8) can be reduced to

$$\pi_e(\omega,q)\simeq\frac{m}{\pi\hbar^2}\left\{1+i\frac{\omega}{qv_F}\frac{\theta[1-(q/2k_F)^2-(\omega/qv_F)^2]}{\sqrt{1-(q/2k_F)^2-(\omega/qv_F)^2}}\right\}. \tag{A1}$$

For comparison, under the same assumptions the polarization function for a 3DEG is given by

$$\pi_e(\omega,q)=\frac{mk_F}{2\pi^2\hbar^2}\left\{1+i\pi\frac{\omega}{qv_F}\theta[1-(q/2k_F)^2-(\omega/qv_F)^2]\right\}, \tag{A2}$$

where $\mathbf{q}=(q_x,q_y,q_z)$ is the bulk wave vector. According to Eq. (5), the inequality $v_F \gg s_{l,t}\sim\omega/q$ holds and the terms with the factor ω/qv_F in Eqs. (A1) and (A2) give a negligible contribution to the absolute value of π_e and $\Delta\varepsilon_e$.

APPENDIX B: LATTICE POLARIZATION

The dielectric function of the system of Fig. 1, defined by Eqs. (11) and (13), is obtained from a solution of Poisson's equation. For $z,z'>0$ one finds

$$\frac{\varepsilon_0}{\varepsilon_s(q;z,z')}=e^{-q|z-z'|}+\frac{\varepsilon_0-1}{\varepsilon_0+1}\,e^{-q(z+z')}. \tag{B1}$$

Substituting Eq. (B1) into Eq. (12), we obtain

$$\frac{1}{\varepsilon_s(q)}=\frac{1}{\varepsilon_0}\left[Z_{\rm bulk}(q)+\frac{\varepsilon_0-1}{\varepsilon_0+1}\,Z_{\rm image}(q)\right], \tag{B2}$$

where the form factors Z are defined in Appendix C.

APPENDIX C: FORM FACTORS

The form factors corresponding to the bulk and image parts of the polarization functions are defined as

$$\left.\begin{matrix}Z_{\rm bulk}(q)\\ Z_{\rm image}(q)\end{matrix}\right\}\equiv\int_0^\infty dz\;\chi^2(z)\int_0^\infty dz'\;\chi^2(z')\begin{cases}\exp(-q|z-z'|)\\ \exp(-q|z+z'|).\end{cases} \tag{C1}$$

The definitions of form factors $\mathcal{Z}(q)$ are obtained from Eq. (C1) after replacement of the exponential functions by cosine functions. We note the relation

$$\mathcal{Z}(q)=\text{Re}\;Z(iq)\;. \tag{C2}$$

Using Eq. (1a), we find for a *square* quantum well ($u\equiv qd$)

$$Z_{\rm bulk}=\frac{(2\pi)^4(e^{-u}-1+u)+20\pi^2\,u^3+3u^5}{u^2[u^2+(2\pi)^2]^2},$$

$$Z_{\rm image}=e^{-2q\ell}\;(2\pi)^4\;\frac{(e^{-u}-1)^2}{u^2[u^2+(2\pi)^2]^2}. \tag{C3}$$

For a *triangular* well, substitution of Eq. (1b) into Eq. (C3) gives ($u\equiv qb$)

$$Z_{\rm bulk}=(8+9\,u+3\,u^2)/8(1+u)^6,$$

$$Z_{\rm image}=e^{-2q\ell}(1+u)^{-6}. \tag{C4}$$

APPENDIX D: BULK ELECTRONS AND PHONONS

For interacting bulk electrons and phonons in a homogeneous system, the momentum and energy relaxation times take the following form, analogous to Eq. (7):

$$\left.\begin{matrix}1/\tau_m\\ 1/\tau_\epsilon\end{matrix}\right\}=\frac{1}{\pi^3\,n_3}\int_0^\infty\frac{d\omega}{\omega^2}\int_0^\infty q^4dq\left\{\begin{matrix}T/3m\\ \omega^2/q^2\end{matrix}\right\}\frac{\text{Im}\;\pi_{\rm ph}(\omega,q)\;\text{Im}\;\pi_e(\omega,q)}{|1+\Delta\varepsilon_e(\omega,q)/\varepsilon_0|^2}\left[\frac{\hbar\omega/2T}{\sinh(\hbar\omega/2T)}\right]^2. \tag{D1}$$

Here $\mathbf{q}=(q_x,q_y,q_z)$ is the three-dimensional transferred wave vector and n_3 is the bulk concentration of electrons. The electron polarization function π_e is given by Lindhard's formula (8) with the system's area $\mathcal{S}$ changed to the system's volume $\mathcal{V}$. Equations (9) and (11) remain intact, but the Fourier image of the Coulomb potential in Eq. (10) takes the three-dimensional form

$$v_{\mathrm{Coul}}(q)=4\pi e^2/q^2. \tag{D2}$$

Finally, for bulk electrons and phonons interacting via the deformation potential coupling, the phonon polarization function is given by

$$\mathrm{Im}\ \pi_{\mathrm{ph}}(\omega,q)=\frac{\Xi^2}{2\rho s_l^2}\,|\omega|\,[\,\delta(\omega-s_l q)-\delta(\omega+s_l q)\,]. \tag{D3}$$

*Present address: Synopsys, Inc., 700 East Middlefield Road, Mountain View, CA 94043.

[1] N. Mori and T. Ando, Phys. Rev. B **40**, 6175 (1989); M. A. Stroscio, *ibid.* **40**, 6428 (1989); L. Wendler, R. Haupt, and V. G. Grigoryan, Physica B **167**, 101 (1990); C. Trallero-Giner, F. Garcia-Moliner, V. R. Velasco, and M. Cardona Phys. Rev. B **45**, 11 944 (1992); M. P. Chamberlain, M. Cardona, and B. K. Ridley, *ibid.* **48**, 14 365 (1993).

[2] M. A. Stroscio *et al.*, in *Properties of III-V Quantum Wells and Superlattices*, edited by P. Bhattacharya (INSPEC, London, 1996), p. 194.

[3] B. A. Auld, *Acoustic Fields and Waves* (Wiley, New York, 1973).

[4] K. F. Graff, *Wave Motion in Elastic Solids* (Clarendon, Oxford, 1975).

[5] M. A. Stroscio, Yu. M. Sirenko, S. Yu, and K. W. Kim, J. Phys. Condens. Matter **8**, 2143 (1996).

[6] R. A. Waldron, IEEE Trans. Microwave Theory Tech. **17**, 893 (1969).

[7] C. Colvard *et al.*, Phys. Rev. B **31**, 2080 (1985); M. V. Klein, IEEE J. Quantum Electron. **22**, 1760 (1986); J. Sapriel and B. Djafari-Rouhani, Surf. Sci. Rep. **10**, 189 (1989); M. W. C. Dharma-Wardana, P. X. Zhang, and D. J. Lockwood Phys. Rev. B **48**, 11 960 (1993).

[8] S. I. Tamura, Phys. Rev. B **43**, 12 646 (1991); S. Mizuno and S. I. Tamura, *ibid.* **45**, 13 423 (1992); N. Nishiguchi, S. I. Tamura, and F. Nori, *ibid.* **48**, 2515 (1993); S. Mizuno, M. Ito, and S. I. Tamura, Jpn. J. Appl. Phys., Part 1 **33**, 2280 (1994); S. Mizuno and S. I. Tamura, *ibid.* **34**, 2556 (1995); A. Yamamoto *et al.*, Phys. Rev. Lett. **73**, 740 (1994).

[9] V. A. Kochelap and O. Gülseren, J. Phys. Condens. Matter **5**, 94 (1993); **5**, 589 (1993).

[10] N. Nishiguchi and T. Sakuma, Solid State Commun. **38**, 1073 (1981); A. Tamura *et al.*, J. Phys. C **15**, 4975 (1982); A. Tamura and T. Ichinokawa, *ibid.* **16**, 4779 (1983).

[11] E. Duval, Phys. Rev. B **46**, 5795 (1992); A. Tanaka *et al.*, *ibid.* **47**, 1237 (1993); S. Saito and T. Goto, *ibid.* **52**, 5929 (1995); N. N. Ovsyuk and V. N. Novikov, Pis'ma Zh. Eksp. Teor. Fiz. **62**, 624 (1995) [JETP Lett. **62**, 647 (1995)]; E. Duval *et al.*, Phys. Rev. Lett. **56**, 2052 (1986); R. W. Schoenlein *et al.*, *ibid.* **70**, 1014 (1993); T. Takagahara, *ibid.* **71**, 3577 (1993).

[12] L. Wendler and V. G. Grigoryan, Surf. Sci. **206**, 203 (1988); V. G. Grigoryan and L. Wendler, Fiz. Tverd. Tela **33**, 2120 (1991) [Sov. Phys. Solid State **33**, 1193 (1991)].

[13] N. Nishiguchi, Jpn. J. Appl. Phys., Part 1 **33**, 2852 (1994); Phys. Rev. B **50**, 10 970 (1994); **52**, 5279 (1995).

[14] Yu. M. Sirenko, M. A. Stroscio, and K. W. Kim, Phys. Rev. E **53**, 1003 (1996); **54**, 1816 (1996).

[15] N. Nishiguchi, Phys. Rev. B **54**, 1494 (1996).

[16] A. K. Viswanath *et al.*, Microw. Opt. Technol. Lett. **7**, 94 (1994); K. Yoh *et al.*, Semicond. Sci. Technol. **9**, 961 (1994).

[17] J. Seyler and M. N. Wybourne, J. Phys. Condens. Matter **4**, L231 (1992); N. Perrin and M. N. Wybourne, Phys. Rev. B **43**, 9511 (1991); J. C. Nabity and M. N. Wybourne, *ibid.* **44**, 8990 (1991); K. Johnson, M. N. Wybourne, and N. Perrin, *ibid.* **50**, 2035 (1994).

[18] M. A. Stroscio, K. W. Kim, S. Yu, and A. Ballato, J. Appl. Phys. **76**, 4670 (1994).

[19] M. A. Stroscio and K. W. Kim, Phys. Rev. B **48**, 1936 (1993); S. Yu, K. W. Kim, M. A. Stroscio, G. J. Iafrate, and A. Ballato, *ibid.* **50**, 1733 (1994); S. Yu, K. W. Kim, M. A. Stroscio, and G. J. Iafrate, *ibid.* **51**, 4695 (1995).

[20] N. Bannov N. V. Mitin, and M. A. Stroscio, Phys. Status Solidi B **183**, 131 (1994); N. Bannov, V. Aristov, and V. Mitin, Solid State Commun. **93**, 483 (1995); N. Bannov, V. Aristov, V. Mitin, and M. A. Stroscio, Phys. Rev. B **51**, 9930 (1995).

[21] M. Feldmann and J. Henaff, *Surface Acoustic Waves for Signal Processing* (Artech, London, 1989).

[22] A. Wixforth, J. P. Kotthaus, and G. Weimann, Phys. Rev. Lett. **56**, 2104 (1986); A. Wixforth *et al.*, Phys. Rev. B **40**, 7874 (1989); V. W. Rampton *et al.*, Semicond. Sci. Technol. **7**, 641 (1992); V. Falko *et al.*, Phys. Rev. B **47**, 9910 (1993); J. P. Pekola *et al.*, *ibid.* **50**, 11 255 (1994); J. M. Shilton *et al.*, *ibid.* **51**, 14 770 (1995).

[23] B. K. Ridley, Semicond. Sci. Technol. **3**, 542 (1988); A. Knäbchen *et al.*, Phys. Rev. B **54**, 10 696 (1996).

[24] R. L. Willett *et al.*, Phys. Rev. Lett. **65**, 112 (1990); J. W. M. Campbell *et al.*, Solid State Commun. **84**, 735 (1992); R. L. Willett *et al.*, Phys. Rev. B **47**, 7344 (1993); Phys. Rev. Lett. **71**, 3846 (1993).

[25] H. Ezawa, S. Kawaji, T. Kuroda, and K. Nakamura, Surf. Sci. **24**, 654 (1971); H. Ezawa, S. Kawaji, and K. Nakamura, *ibid.* **27**, 218 (1971); S. Kawaji, H. Ezawa, and K. Nakamura, J. Vac. Sci. Technol. **9**, 762 (1972); H. Ezawa, Surf. Sci. **58**, 25 (1976).

[26] H. Ezawa, Ann. Phys. (N.Y.) **67**, 438 (1971).

[27] H. Ezawa, S. Kawaji, and K. Nakamura, Jpn. J. Appl. Phys. **13**, 126 (1974).

[28] X. L. Lei and C. S. Ting, Phys. Rev. B **32**, 1112 (1985); N. J. M. Horing, X. L. Lei, and H. L. Cui, *ibid.* **33**, 6929 (1986); X. L. Lei, N. J. M. Horing, and J. Q. Zhang, *ibid.* **34**, 1139 (1986); X. L. Lei, H. L. Cui, and N. J. M. Horing, *ibid.* **38**, 8230 (1988).

[29] I. I. Boiko and Yu. M. Sirenko, Zh. Tekh. Fiz. **58**, 967 (1988) [Sov. Phys. Tech. Phys. **33**, 586 (1988)]; Ukr. Phys. J. **33**, 1560 (1988); Phys. Status Solidi B **159**, 805 (1991); I. I. Boiko, Yu. M. Sirenko, and P. Vasilopoulos, Phys. Rev. B **43**, 7216 (1991); **43**, 7224 (1991); Yu. M. Sirenko, P. Vasilopoulos, and I. I. Boiko, *ibid.* **44**, 10 724 (1991); I. I. Boiko, P. Vasilopoulos, and Yu. M. Sirenko, *ibid.* **45**, 13 538 (1992); Yu. M. Sirenko and P. Vasilopoulos, Superlattices Microstruct. **12**, 403 (1992); Phys. Rev. B **46**, 1611 (1992).

[30] J. K. Jain, R. Jalabert, and S. Das Sarma, Phys. Rev. Lett. **60**, 353

(1988); S. Das Sarma, J. K. Jain, and R. Jalabert, Phys. Rev. B **37**, 4560 (1988); **37**, 6290 (1988); **41**, 3561 (1990).

[31] V. T. Nguyen and G. Mahler, Phys. Rev. B **45**, 4151 (1992).

[32] B. A. Sanborn, Phys. Rev. B **51**, 14 247 (1995); **51**, 14 256 (1995).

[33] Cubic materials are characterized by three independent components C_{11}, C_{12}, and C_{44} of elastic stiffness matrix C. In the isotropic approximation (Ref. 34) the following two independent components lead to the best least-squares approximation for the sound velocities: $\overline{C_{11}}=C_{11}-2\Delta$ and $\overline{C_{44}}=C_{44}+\Delta$, where $\Delta=(C_{11}-C_{12}-2C_{44})/5$. Averaged longitudinal and transverse sound velocities are given by $s_l^2=\overline{C_{11}}/\rho$ and $s_t^2=\overline{C_{44}}/\rho$, where ρ is a crystal density.

[34] F. I. Fedorov, *Theory of Elastic Waves in Crystals* (Plenum, New York, 1968).

[35] V. F. Gantmakher and Y. B. Levinson, *Carrier Scattering in Metals and Semiconductors* (North-Holland, Amsterdam, 1987).

[36] The phonon frequency is denoted by the uppercase letter Ω to distinguish it from a dummy variable ω in Eq. (7), corresponding to the transferred energy. The choice of Ω as one of the phonon quantum numbers is more convenient than the ''in-plane phase velocity'' $c\equiv\Omega/q$ defined by Ezawa (Ref. 26). We also use the incident longitudinal/transverse waves representation in Eqs. (20) and (23) instead of the symmetrized forms used in Ref. 26.

[37] L. D. Landau and E. M. Lifshitz, *Statistical Physics* (Pergamon, Oxford, 1980).

[38] In fact, the cutoff at $\omega\lesssim q\overline{v}$ is not effective due to the assumption $s\ll\overline{v}$ in Eq. (5).

[39] V. Karpus, Fiz. Tekh. Poluprovodn. **20**, 12 (1986) [Sov. Phys. Semicond. **20**, 6 (1986)]; Semicond. Sci. Technol. **5**, 691 (1990).

[40] I. I. Boiko and Yu. M. Sirenko, Phys. Status Solidi B **159**, K37 (1991).

[41] V. Karpus, Fiz. Tekh. Poluprovodn. **21**, 1949 (1987) [Sov. Phys. Semicond. **21**, 1180 (1987)]; **22**, 439 (1988); [**22**, 268 (1988)].

[42] *Numerical Data and Functional Relationships in Science and Technology* , Group III, Vol. 17 Pt. a, edited by O. Madelung (Springer, Berlin, 1982).

[43] The average electron coordinate $\langle z-\not{z}\rangle$ is equal to $d/2$ for a square quantum well and $3/b$ for a triangular quantum well, leading to the correspondence rule $d\rightarrow 6/b$.